Catalysis
Science &
Technology

This article can be cited before page numbers have been issued, to do this please use: W. Gong, C. Chen, H. Zhang, G. Wang and H. Zhao, *Catal. Sci. Technol.*, 2018, DOI: 10.1039/C8CY01488D.

View Article Online
DOI: 10.1039/C8CY01488D

Journal Name

ARTICLE

Received 00th January 20xx,
Accepted 00th January 20xx

DOI: 10.1039/x0xx00000x

www.rsc.org/

Highly dispersed Co, Ni nanoparticles encapsulated in N-doped carbon nanotubes as efficient catalysts for reduction of unsaturated oxygen compounds in aqueous-phase

Wanbing Gong,[a] Chun Chen,*[a] Haimin Zhang,[a] Guozhong Wang[a] and Huijun Zhao*[ab]

N-doped carbon nanotubes encapsulated metal nanoparticles are of great interest in heterogeneous catalysis owing to their improved mass transfer ability and superior stability. Herein, a facile one-pot pyrolysis approach using melamine as carbon and nitrogen source was developed to fabricate metal nanoparticles embedded in bamboo-like N-doped carbon nanotubes (named as Co@NCNTs-600-800 and Ni@NCNTs-600-800). The optimized Co@NCNTs-600-800 catalyst exhibited outstanding activity in furfural (FAL) selective hydrogenation to furfuryl alcohol (FOL) or cyclopentanone (CPO) in aqueous media. The high yields of FOL (100%) and CPO (75.3%) were achieved at 80 °C and 140 °C, respectively. Besides, this cobalt catalyst showed very good stability and recyclability during the reaction. The synergistic effect between metallic cobalt and N-doped carbon nanotubes was systematically investigated. In addition, the as-prepared Ni@NCNTs-600-800 catalyst also exhibited remarkable activity. Under the optimal conditions (100 °C and 4 MPa H_2 pressure), a maximum tetrahydrofurfuryl alcohol (THFOL) yield (99.5%) was obtained in the aqueous-phase hydrogenation of FAL. The research thus highlights new perspectives for non-noble metal-based N-doped carbon nanotubes catalysts for biomass transformation.

1. Introduction

Due to the decrease of fossil fuel sources and the increase of environmental pollution, the catalytic conversion of bio-refinery platform molecules to fuels and value-added chemicals has been the subject of intense research in the recent years.[1-3] Especially, furfural (FAL) is one of these promising platform molecules, and it is produced easily and commercially by combined acid-catalyzed hydrolysis and the dehydration of hemicellulosic xylans in lignocellulose.[4, 5] FAL can be further converted into many valuable chemicals, such as furfuryl alcohol (FOL), tetrahydrofurfuryl alcohol (THFOL), 2-methylfuran (2-MF), cyclopentanone (CPO) and cyclopentanol (CPL) by the hydrogenation or hydrodeoxygenation way.[6, 7] Among these products, the as-synthesized alcohols have been extensively used in industrial processes as green solvents or intermediates for fine chemical synthesis, such as resins, fibers and wetting agents.[7, 8] For instance, CPO is a versatile compound used for the synthesis of fuels, fungicides, pharmaceuticals, rubber chemicals, and flavor and fragrance chemicals.[5, 9] The catalytic hydrogenation of FAL to these chemicals is carried out either in the gas-phase or in the liquid-phase.[10] The gas-phase hydrogenation can suffer from poor selectivity of target products or catalyst deactivation.[11] To overcome the mentioned shortcomings, it is attractive to design an efficient catalysis system for FAL hydrogenation in liquid-phase. Strikingly, the conventional liquid-phase hydrogenation is not eco-friendly because it inevitably requires organic solvents (methanol, ethanol or 2-propanol) or produces toxic wastes.[12, 13] From the standpoint of green chemistry, the use of water as reaction medium is preferred.[14] Despite the number of investigations in liquid-phase hydrogenation of FAL, there are not much references about the selective hydrogenation of FAL in aqueous-phase.[6] Recently, several research groups have done some pioneering works in this regard. For example, Pd–Cu supported on MgO or $Mg(OH)_2$ exhibited complete conversion and higher than 98% selectivity at 110 °C and 0.6 MPa of hydrogen in aqueous-phase hydrogenation of FAL to FOL.[15] Chen et al. also reported complete conversion and high selectivity (> 99%) in water was observed for g-C_3N_4 nanosheets supported Pt catalysts at 100 °C after 5 h reaction.[14] Yang et al. found the FAL was almost completely converted to THFOL over Ni/Ba–Al_2O_3 in water under optimized conditions (140 °C, 4 MPa H_2 and 4 h).[16] At present, more and more research groups have focused on the study of aqueous-phase hydrogenation of FAL to CPO. About 98% FAL conversion with 92.1 mol% CPO yield were early reported under an optimal condition (160 °C, 3 MPa of hydrogen) over Pd–Cu catalyst.[17] Later, Guo et al. demonstrated that a 62% yield of CPO was obtained at the optimized condition (150 °C, 4 MPa H_2, 6 h) over CuZnAl

---

[a] Key Laboratory of Materials Physics, Centre for Environmental and Energy Nanomaterials, Anhui Key Laboratory of Nanomaterials and Nanotechnology, CAS Centre for Excellence in Nanoscience, Institute of Solid State Physics, Chinese Academy of Sciences, Hefei 230031, P. R. China. E-mail: h.zhao@griffith.edu.au, chenchun2013@issp.ac.cn.

[b] Centre for Clean Environment and Energy, Gold Coast Campus, Griffith University, Queensland 4222, Australia

†Electronic Supplementary Information (ESI) available. See DOI: 10.1039/x0xx00000x

View Article Online
DOI: 10.1039/C8CY01488D

catalyst.[18] Recently, 95% FAL conversion with 85% CPO yield was achieved over a CuZn/CNT catalyst in a mild reaction condition (140 ^{o}C, 4 MPa H_2).[19] Although some promising works have been done on the hydrogenation of biomass-derived FAL to some valuable chemicals using water as solvent, further studies are still needed in developing non-noble metal based catalysts with excellent catalytic performance under mild reaction condition.

In recent years, tremendous efforts have been made to develop novel N-doped carbon based materials due to their desirable physical and chemical properties.[20, 21] As catalysts or supports, N-doped carbon based materials have shown superior activities in many applications covering a wide range of heterogeneous catalytic reactions.[22, 23] Among them, metal nanoparticles encapsulated in N-doped carbon nanotubes (NCNTs) are widely used to improve the performance of the catalysts because of high electron transfer performance and abundant active sites.[24-26] For example, Cao et al. developed a facile synthesis method for N-doped bamboo-like carbon nanotubes (CNTs) with Co nanoparticles encapsulated at the tips. The uniform catalyst showed better ORR catalytic activity and higher stability in alkaline solutions compared with commercial Pt/C and comparable catalytic activity to Pt/C in acidic media.[27] Recently, Lin et al. reported the facile synthesis of cobalt nanoparticles encapsulated into graphitic N-doped carbon nanotube materials. The composites showed excellent catalytical performance for selective oxidation of ethylbenzene under solvent-free and molecular oxygen conditions.[28] However, to the best of our knowledge, metal nanoparticles encapsulated in N-doped carbon nanotubes are rarely applied to selectively catalytic aqueous-phase hydrogenation reactions.

Herein, we report a facile approach to fabricate metal nanoparticles embedded bamboo-like N-doped carbon nanotubes (named as Co@NCNTs-600-800/ Ni@NCNTs-600-800) via thermolysis of melamine and corresponding nitrates ($Co(NO_3)_2{\cdot}6H_2O$ or $Ni(NO_3)_2{\cdot}6H_2O$). The samples have been characterized by SEM, TEM, STEM, XRD, XPS, Raman and BET. The Co@NCNTs-600-800 exhibited an excellent catalytic performance for selective hydrogenation of FAL to FOL and CPO in aqueous-phase under mild conditions, respectively. The excellent stability of catalyst was also proved. Besides, the Ni@NCNTs-600-800 was demonstrated to be an effective catalyst for aqueous-phase hydrogenation of FAL to THFOL.

2. Experimental

2.1. Materials and Chemicals

$Co(NO_3)_2{\cdot}6H_2O$, $Ni(NO_3)_2{\cdot}6H_2O$ and melamine were purchased from Sinopharm Chemical Reagent Co. Ltd. FAL (99%), FOL (98%), THFOL (98%), CPO (99.5%), CPL (99.5%), n-octanol (99.5%) and ethyl acetate (99%) were purchased from Aladdin Reagent Company. Other analytical grade solvents including ethanol were commercially available.

2.2. Catalyst preparation

In a typical synthesis, 0.003 mol of $Co(NO_3)_2{\cdot}6H_2O$ was first dissolved in an appropriate amount of ethanol. Then, 0.012 mol of melamine was added into the above solution and continually stirred for 0.5 h. Next, the homogeneous mixture was stirred at room temperature until ethanol was fully evaporated and dried at 60 ^{o}C overnight. Afterward, the mixture was transferred into a ceramic boat and heated to 600 °C for 2 h with a ramp rate of 2 ^{o}C min^{-1} under a N_2 flow (first step heat treatment), and the temperature further rose to desired temperature for 2 h with a ramp rate of 4 ^{o}C min^{-1} under a N_2 atmosphere (second step heat treatment). Finally, the sample was gained by cooling down to room temperature. The obtained sample was denoted Co@NCNTs-600-x (x stands for the temperature in the second step heat treatment). For comparison, Co@NC-600 was also synthesized without high temperature treatment in the second step. Similarly, the Ni@NCNTs-600-x samples were also prepared by the identical synthesis strategy in which the metal salt was substituted by $Ni(NO_3)_2{\cdot}6H_2O$.

2.3. Catalyst characterization

Field emission scanning electron microscopy (FESEM) images of the samples were taken on a FESEM (SU8020) operated at an accelerating voltage of 10.0 kV. Transmission electron microscopy (TEM, JEOL-2010) images operated at an acceleration voltage of 200 kV. Scanning transmission electron microscopy (STEM) images of the samples were recorded by a high resolution TEM (Philips TecnaiG2 F20) operated at an acceleration voltage of 200 kV. Powder X-ray diffraction (XRD) patterns were analyzed on a Philips X-Pert Pro X-ray diffractometer with using the Ni-filtered monochromatic Cu Kα radiation ($\lambda K_{\alpha1}$ = 1.5418 Å) at 40 keV and 40 mA. The surface area and porosity of samples were measured at 77 K using a Surface Area and Porosity Analyzer (Autosorb iQ Station 2). XPS analysis was performed on an ESCALAB 250 X-ray photoelectron spectrometer (Thermo, USA) equipped with Al $K_{\alpha1,2}$ monochromatized radiation at 1486.6 eV X-ray source. Raman spectra of the samples were recorded on a LabRAM HR800 confocal microscope Raman system (Horiba Jobin Yvon) using an Ar ion laser operating at 632 nm. The metal content in the composite structure was determined by the inductively coupled plasma spectroscopy after microwave digestion of the samples (ICP 6300, Thermo Fisher Scientific).

2.4. Catalytic tests

The catalytic hydrogenation of FAL was carried out in a 25 mL stainless steel autoclave with a mechanical stirrer, a pressure gauge and automatic temperature control apparatus. In a typical experiment, the reaction solutions of FAL (1 mmol), catalyst (30 mg), and H_2O (10 ml) were loaded into the reactor. The reactor was sealed, purged three times with N_2 at 1 MPa, and then pressurized with H_2 to a setting point. The reactor was then heated to the desired temperature and the stirring speed fixed to 700 rpm which eliminates the diffusion effects. After reaction, the autoclave was cooled down quickly. The autoclave contents were transferred to a centrifuge tube, and the catalyst was separated by centrifugation.

View Article Online
DOI: 10.1039/C8CY01488D

The products were extracted by ethyl acetate from the liquid and then analyzed.

The liquid product was identified by gas chromatography–mass spectrometry (GC-MS, Thermo Fisher Scientific-TXQ Quntum XLS, column-TG-WAXMS, 30 m × 0.25 mm × 0.25 μm), and was quantitatively analyzed by GC (Shimadzu, GC-2010 Plus), equipped with FID and a (30 m × 0.25 mm × 0.25 μm) KB-WAX capillary column (Kromat Corporation, USA) using n-octanol as an internal standard. The carbon balance was checked in every run and it was found to be higher than 94%.

During the catalyst stability test, the catalyst was reused without any further treatments. More specifically, the reaction mixture was filtered to recover the catalyst, which was washed first with acetone then water followed by drying under vacuum oven at 60 ^{o}C and employed for stability test.

3. Results and discussions

The preparation procedure for the Co@NCNTs-600-800 catalyst is briefly illustrated in Fig. 1a, where the melamine acts as carbon and nitrogen source. The synthesis started with the formation of Co@NC-600 by heat treatment at 600 ^{o}C, which was consisted of irregular short rods (Fig. 1b). Then, the Co@NC-600 was subjected to high-temperature pyrolysis at 800 ^{o}C under N_2 atmosphere to yield the desired Co@NCNTs-600-800. Finally, the N-doped carbon nanotubes with lengths of more than several micrometers was formed, a closer look showed that white dots were found at the tip of N-doped carbon nanotubes, indicating that the incorporation of Co nanoparticles when the sample was further treated at high temperature (Fig. 1c). The TEM image (Fig. 1d) of Co@NCNTs-600-800 observes the typical bamboo-like N-doped carbon nanotubes with diameters ranging from 30 to 40 nm were formed, and cobalt nanoparticles were encapsulated at the tip of nanotubes. The HRTEM (Fig. 1e) and HAADF-STEM images (Fig. 1f) further confirm Co nanoparticles were coated by thin graphitic carbon layers, and the wall thickness was only about 2-4 nm. The lattice fringe of the core was consistent with the Co crystal structure having (111) lattice fringes with an interspacing of 0.204 nm. The corresponding elemental mapping from HAADF-STEM image (Fig. 1g) shows that Co, O, N and C were homogeneously distributed on the catalyst.

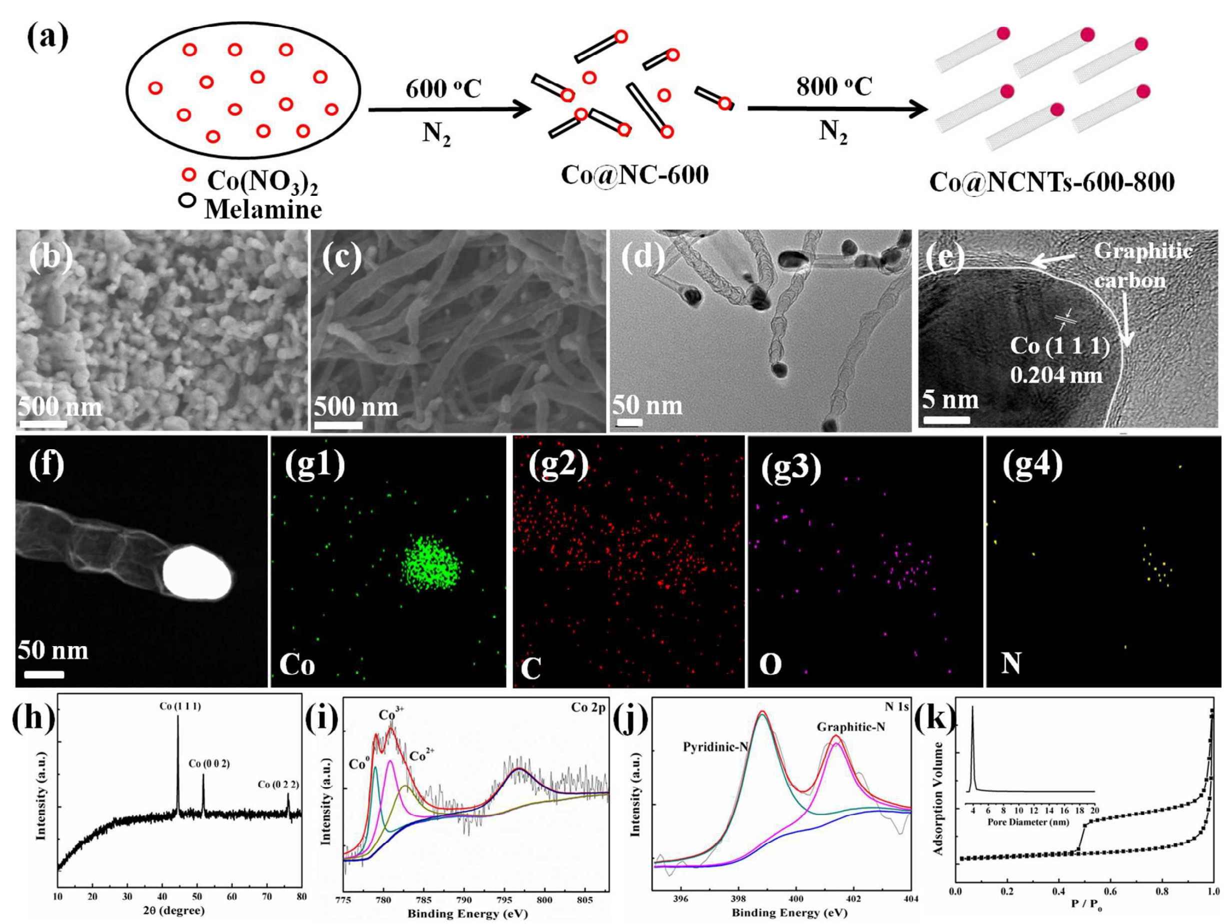

Fig. 1 (a) Schematic illustration of the synthetic procedure of the Co catalysts; (b) SEM image of as-prepared Co@NC-600; (c) SEM image, (d) TEM image, (e) HRTEM image, (f) HAADF-STEM image, (g) EDX mapping, (h) XRD pattern, (i) Co 2p spectrum, (j) N 1s spectrum, (k) N_2 adsorption and desorption isotherm and BJH pore size distribution plot (inset) of as-prepared Co@NCNTs-600-800.

View Article Online
DOI: 10.1039/C8CY01488D

The XRD diffraction pattern (Fig. 1h) displays three peaks at 44.2°, 51.5°, and 75.9°, corresponding to (111), (002), and (022) of cubic Co (JCPDS 96-901-0969), respectively. XPS characterization is carried out to identify the surface electronic states of the catalyst. The surface XPS survey spectrum (Fig. S1a†) shows the sample was mainly composed of C (92.2 at.%), O (3.31 at.%), N (3.83 at.%) and Co (0.67 at.%). The low Co content was due to that Co nanoparticles were tightly encapsulated by thin carbon layers in the catalyst.[27] The characteristic Co $2p_{3/2}$ and Co $2p_{1/2}$ peaks related to the spin-orbit splitting are observed from the high resolution Co 2p spectrum (Fig. 1i), and Co $2p_{3/2}$ was fitted into Co^0, Co^{3+}, Co^{2+} and satellites peaks, which confirmed the mixture of Co^0 and CoO_x on the surface of catalyst.[28] In the meantime, the high resolution N 1s spectrum (Fig. 1j) was fitted into two peaks at 398.7 eV for pyridinic N (N1) and 401.3 eV for graphic N (N3), indicating the successful incorporation of N into the carbon nanotubes.[29] The high N doping content (3.83 at.%), high percentage of pyridinic N (67.5 %), and certain percentage of graphitic N (32.5 %) in the Co@NCNTs-600-800 were beneficial to improving the aqueous-phase hydrogenation activity (Table S1†). Nitrogen adsorption–desorption isotherms measured at 77 K are used to evaluate the specific surface areas and porous structures of samples. The sample exhibited type-IV isotherms with hysteresis loops, indicating the presence of mesoporous structures (Fig. 1k). The specific surface area and total pore volume were 200.7 m^2 g^{-1} and 0.588 cm^3 g^{-1} (Table S1†), respectively. The ICP data shows the Co content was 40.3 wt% for Co@NCNTs-600-800 (Table S1†). The high content of metallic Co can enhance the catalytic activities for N-doped porous carbon materials. Based on the above results, the metallic Co nanoparticles encapsulated by N-doped carbon nanotubes play an important role in the remarkable catalytic activity for the aqueous-phase reactions.

The selective aqueous-phase hydrogenation of FAL to CPO is chosen as the model reaction to evaluate the catalytic performance of as-prepared Co@NCNTs-600-800 catalyst. Fig. 2a demonstrates that FAL conversion gradually increased from 22.9% at 60 °C to almost 100% at 130 °C at 4 MPa H_2 pressure after 5 h reaction. The main products were FOL, CPO and CPL. At the low temperature range (60-80 °C), FOL was sole product. After that, it is found that CPO selectivity raised from 0.8% to 75.3% with reaction temperature increased from 90 to 140 °C. But then the CPO selectivity decreased to 75.1% at 160 °C because of the deep hydrogenation of CPO to CPL. In addition, the reaction time

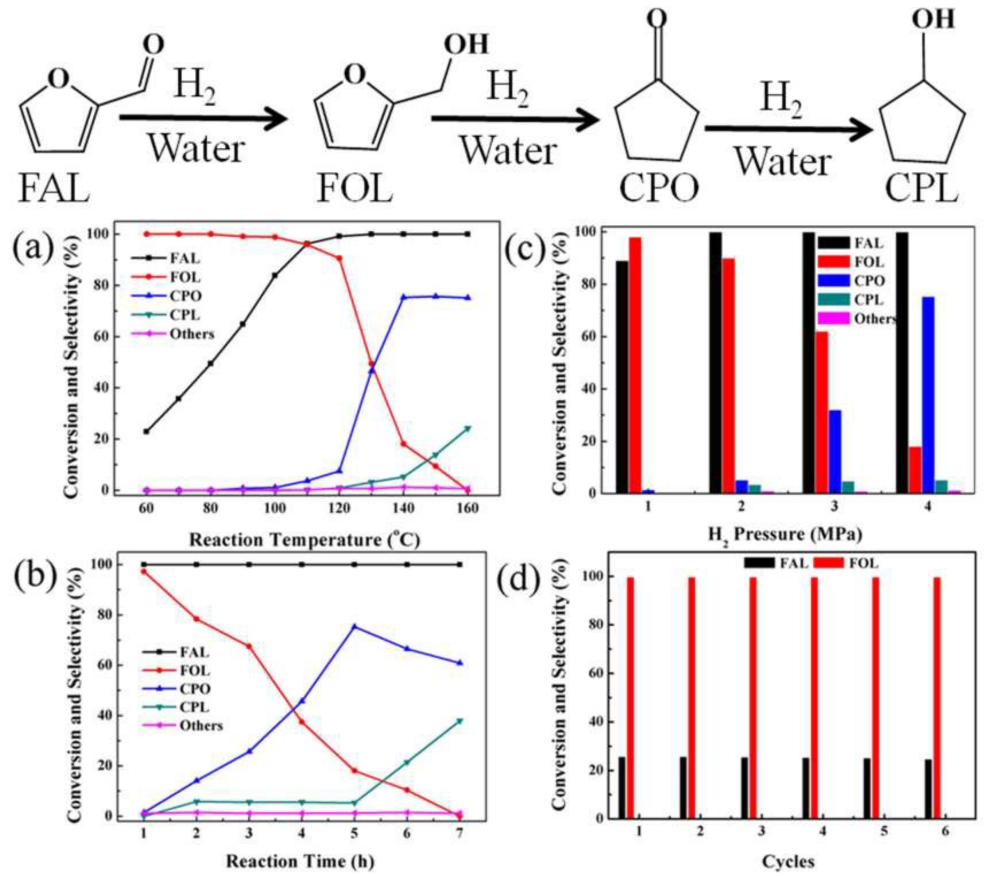

Fig. 2 Aqueous hydrogenation of FAL over Co@NCNTs-600-800. Reaction conditions: (a) Catalyst = 30 mg, FAL = 1 mmol, Water =10 mL, H_2 pressure = 4 MPa, Reaction time = 5 h. (b) Catalyst = 30 mg, FAL = 1 mmol, Water =10 mL, Reaction temperature = 140 °C, H_2 pressure = 4 MPa. (c) Catalyst = 30 mg, FAL = 1 mmol, Water =10 mL, Reaction temperature = 140 °C, Reaction time = 5 h. (d) Catalyst = 30 mg, FAL = 1 mmol, Water =10 mL, Reaction temperature = 80 °C, H_2 pressure = 4 MPa, Reaction time = 3 h.

DOI: 10.1039/C8CY01488D

dependence of FAL hydrogenation on Co@NCNTs-600-800 was also surveyed. Firstly, the FAL conversion gradually increased from 7.6% within 1 h to 49.5% within 5 h at the low temperature of 80 °C (Fig. S2†). When the reaction time was extended to 8 h, almost complete conversion was definitively obtained. Fig. 2b further shows that the selectivity of FOL decreased and CPO/CPL selectivity increased as reaction time went on at the high temperature of 140 °C. After 1 hour reaction, almost 100% FAL conversion with 97.3% FOL selectivity and 1.5% CPO selectivity were achieved. Then CPO selectivity increased from 14.1% to 75.3% as reaction time increased from 2 h to 5 h. After 7 h reaction, the CPO selectivity decreased to 60.9%. It is attributed to the overreaction in hydrogenation of CPO to CPL, which causes a decrease of CPO selectivity but increase of the corresponding CPL selectivity. Based on these data, in order to gain high CPO selectivity in the aqueous-phase hydrogenation of FAL, the reactant is first transformed to FOL and then the intermediate is further hydrogenated to CPO rather than THFOL in the presence of water reaction medium. The result is consistent with the previous studies.[9, 17] To further study structural change of the catalyst, the XRD patterns of the catalyst with different reaction time were demonstrated (Fig. S3†). It reveals the structure of the catalyst remained unchanged, but intensity of the metal peaks gradually weakened with the prolonging of reaction time, indicating the catalyst could be oxidized gradually in medium of water under reaction condition. To provide more insights into the aqueous-phase hydrogenation of FAL into CPO, the rate constants *k* at different temperatures can be calculated over the Co@NCNTs-600-800 catalyst and the results are shown in Fig. S4†. The aqueous-phase hydrogenation of FAL showed pseudo-first-order kinetics for all studied temperatures at the condition of low conversion. The rate constants *k* were 0.0117 min^{-1}, 0.0172 min^{-1}, 0.0202 min^{-1} and 0.0259 min^{-1} for temperatures of 120 °C, 130 °C, 140 °C and 150 °C, respectively. Moreover, the rate constants for the hydrogenation of FAL to FOL are much higher than that for generating CPO, indicating that the step of FOL to CPO is the rate-determining step. According to the Arrhenius plots at the low conversion of FAL, the activation energy (*Ea*) was calculated to be 34 kJ mol^{-1} over the Co@NCNTs-600-800 catalyst (Fig. S5†). Moreover, the TOF values were also calculated to investigate the intrinsic catalytic activity in a low conversion. The calculated TOF values were 231 h^{-1}, 285 h^{-1}, 339 h^{-1} and 428 h^{-1} for temperatures of 120 °C, 130 °C, 140 °C and 150 °C over the Co@NCNTs-600-800 catalyst, respectively (Table S2†). Fig. 2c shows the catalytic performance of aqueous-phase FAL hydrogenation by varying H_2 pressure. At relatively low H_2 pressure (1 MPa), the FAL conversion was 89.1%, and the selectivity of FOL and CPO were 98.1% and 1.5%, respectively. When the H_2 pressure increased to 4 MPa, FAL was completely converted and CPO selectivity was 75.3%.

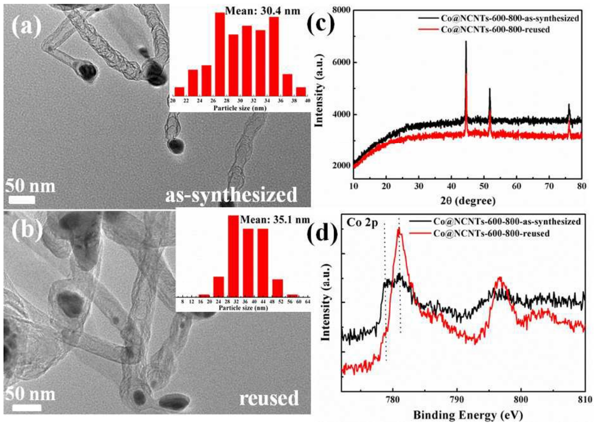

Fig. 3 (a-b) TEM images, (c) XRD patterns and (d) Co 2p spectrums of the as-synthesized and reused Co@NCNTs-600-800 catalysts. The inset in (a-b) shows the distribution of corresponding particle size.

Lastly, we evaluated the recyclability of Co@NCNTs-600-800 catalyst at low conversion (~ 25 %), and the results are shown in Fig. 2d. The FAL conversion remained almost unchanged after six cycles, indicating the good stability of the catalyst. The reused catalyst had been characterized by ICP, TEM, XRD and XPS. As determined by ICP technique, the Co content in the reused catalyst is 17.0 wt%, which is closed to 17.2 wt% in the as-synthesized catalyst, and only trace amount of Co has been detected in the reaction mixture after six cycle runs. is known that leaching or sintering of active metal is a key obstacle for heterogeneous metal catalysts in a water medium. The obtained Co@NCNTs-600-800 catalyst displayed high stability due to the protecting effect of N-doped carbon shell. The cobalt particles had a certain aggregation and the average particle size increased from 30.4 nm to 35.1 nm after six runs (Fig. 3a-b). The intensities of cobalt peaks decreased slightly after six runs, which could be attributed to active sites were gradually oxidized (Fig. 3c). For deeply confirming the changes of Co catalyst in reaction, the chemical state of reused catalyst was determined by XPS analysis (Fig. 3d). Comparing with the fresh catalyst, the content of cobalt was basically the same (0.66 at.%), and cobalt oxides (CoOx) have been detected obviously after six runs. It indicates that the metallic Co NPs on the surface of support could be oxidized under reaction conditions.

The above results demonstrate superior aqueous-phase hydrogenation catalytic performances of the as-synthesized Co@NCNTs-600-800 catalyst. To further understand the

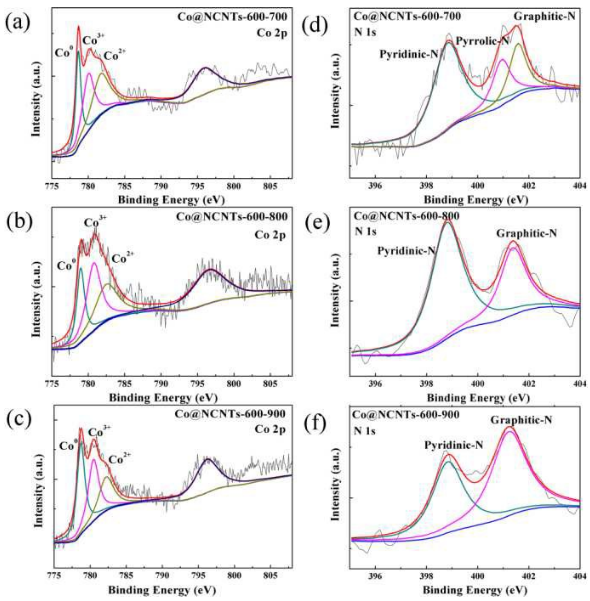

Fig. 4 Co 2p (a-c) and N 1s (d-f) XPS spectrum of Co@NCNTs-600-700, Co@NCNTs-600-800 and Co@NCNTs-600-900 catalysts.

View Article Online
DOI: 10.1039/C8CY01488D

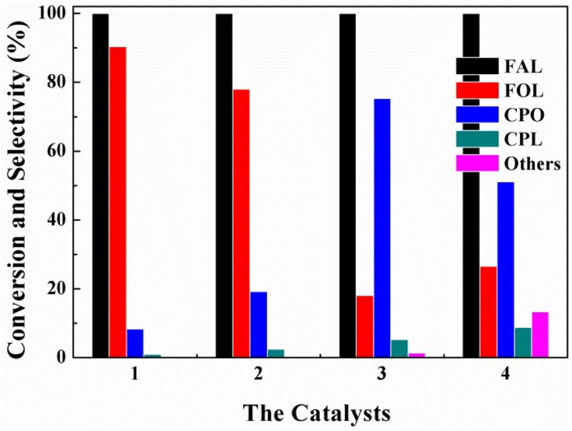

Fig. 5 Hydrogenation of FAL over different Co catalysts. 1, Co@NC-600; 2, Co@NCNTs-600-700; 3, Co@NCNTs-600-800; 4, Co@NCNTs-600-900. (Reaction conditions: Catalyst = 30 mg, FAL = 1 mmol, Water =10 mL, Reaction temperature = 140 °C, H_2 pressure = 4 MPa, Reaction time = 5 h.)

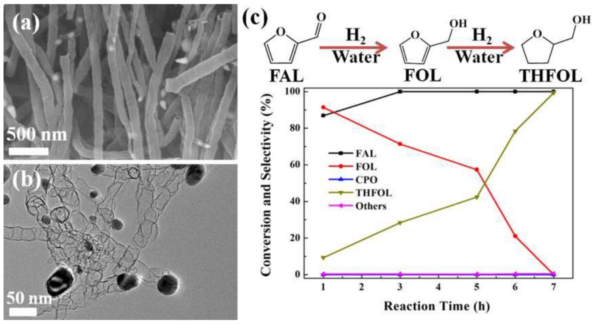

Fig. 6 Characterization and evaluation of Ni@NCNTs-600-800: (a) SEM image; (b) TEM image; (c) effect of reaction time on the hydrogenation of FAL. (Reaction conditions: Catalyst = 30 mg, FAL = 1 mmol, Water =10 mL, Reaction temperature = 100 °C, H_2 pressure = 4 MPa.)

relationship between the structure and activity of the as-synthesized cobalt catalysts, different Co based catalysts were synthesized and evaluated. On the basis of XRD analysis (Fig. S6†), it clearly shows that the diffraction peaks of metallic cobalt were apparently more intense and sharp with the increase of calcination temperature, indicating a higher crystallization and crystallite size at an elevated temperature. The mean size of Co nanoparticles were about 21.4 nm, 28.6 nm and 52.1 nm (based on Scherrer equation) for Co@NCNTs-600-700, Co@NCNTs-600-800 and Co@NCNTs-600-900 catalysts, respectively (Table S1†). Besides, the Raman spectrum (Fig. S7†) shows that two peaks located at about 1350 cm^{-1} and 1580 cm^{-1} can be assigned to typical D- and G-bands of carbon, respectively.[30] The relative intensity ratio of D-band to G-band (I_D/I_G) was decreased with the increase of calcination temperature, indicating a higher degree of graphitization. The SEM images (Fig. S8†) show that tubular morphology and structure became more and more uniform with the increase of calcination temperature from the 700 °C to 800 °C. But irregular and broken tubular morphology has also been found when the temperature was further increased to 900 °C, which suggests that 800 °C is optimum calcination temperature to form highly ordered tubular morphology. Besides, the diameters of the nanotubes increased with calcination temperature (Fig. S9†). The specific surface area and total pore volume increased with the increasing of calcination temperature from 700 °C to 800 °C. It can be attributed to the formation of N-doped carbon nanotubes at elevated temperature.[28] However, when the temperature was further increased to 900 °C, the larger Co nanoparticles and broken tubular morphology were inevitably formed (Table S1 and Fig. S10, †). The average pore diameter was basically the same (~ 3.9 nm) for all samples (Fig. S10†). In terms of the chemical environment and electronic structure of surface, Fig. 4 shows Co 2p and N 1s XPS spectrum of different Co catalysts. According to the fitting results, with the increasing calcination temperature from 700 °C to 900 °C, the proportion of metallic Co increased, indicating that the extent of reduction of cobalt ions was higher on the surface of catalysts (Table S1†). Moreover, we can find that the N doping content increased first then decreased with the calcination temperature (Table S1†). In terms of N types, pyridinic N was the dominant phase in the Co@NCNTs-600-700 and Co@NCNTs-600-800, but graphitic N became the dominant phase in the Co@NCNTs-600-900 catalyst. It can be inferred from Fig. 4 that the conversion of pyridinic N and pyrrolic N (400.8 eV, N2) to graphitic N can occur gradually with the increase of calcination temperature. Some studies had also confirmed that pyridinic N can effectively contribute the carbon material surface with Lewis base property, possibly being favourable for the adsorption of acidic functional groups or precursors on material surface, thus improving catalytic performance.[31, 32] Moreover, graphitic N in carbon based catalysts can effectively improve their electron transfer capability, thus resulting in high catalytic performance in hydrogenation.[33] In our previous work, we suggested that pyridinic N can make carbon with Lewis basic sites to increase the dispersion of catalyst in solvent and adsorption of FAL. Meanwhile, graphitic N could effectively increased the electron transfer property of catalyst, thus improving the catalytical hydrogenation performance.[34] The O 1s peak (Fig. S1b-d†) suggests the presence of three main O-containing species: the lattice oxygen species (O1, ~ 530.2 eV), surface oxygen species (O2, ~ 531.8 eV) and adsorbed oxygen species (O3, ~ 533.2 eV).[35, 36] It can be found that relative amount of surface defects (i.e. oxygen vacancies) were existed on the surface of catalyst. These results provide basic clues concerning the interaction between the Co and N-doped carbon nanotubes.

Several supported Co catalysts were screened for the aqueous-phase hydrogenation of FAL, and their activity results are shown in detail. First, FOL was identified as sole product obtained from FAL hydrogenation at the low temperature of 80 °C after 5 h reaction (Fig. S11†), indicating that the cobalt is a truly selective hydrogenation catalyst for the C=O bond of unsaturated aldehydes.[37, 38] Besides, we can find that the FAL conversion increased first then decreased with the calcination temperature increased from 600 °C to 900 °C. When using Co@NCNTs-600-800 as catalyst, the highest FAL conversion (49.5%) to FOL can be achieved at 80 °C after 5 h reaction. Next, the FAL can be further converted to CPO through furan ring rearrangement at high temperature in aqueous medium generally.[18, 39] Fig. 5 exhibits FAL can be hydrogenated to CPO at the high temperature of 140 °C. In

View Article Online
DOI: 10.1039/C8CY01488D

all cases, the full conversion was obtained after 5 h reaction under 4 MPa H_2 pressure. Due to the unaffected C=C bond and the easier hydrogenation of the C=O bond to an alcohol, the major product was consisted of the FOL and CPO. With the increase of calcination temperature, the CPO selectivity increased first then decreased. And a 75.3% CPO selectivity with complete conversion was realized within 5 h using Co@NCNTs-600-800 as catalyst. These experiments directly confirm that Co@NCNTs-600-800 is the optimum catalyst for the hydrogenation of FAL to FOL and CPO, respectively.

Based on the above experimental results and previous discussions, the possible main reasons for their high activity and selectivity in this work could be attributed to the synergistic effect of following points: (1) abundant graphited carbon nanotubes with high surface area can give rise to abundant active sites; (2) high N-doping content and appropriate N-doping type can increase adsorption of FAL and electron transfer; (3) highly dispersed Co nanoparticles can increase the activation of H_2 and FAL; (4) the synergy between Co nanoparticles and graphited N-doped carbon nanotubes can enhance the hydrogenation of FAL. After etching with 2 M HCl solution, the intensities of metallic Co peaks decreased sharply (Fig. S12†), suggesting the metallic Co NPs on the surface of support have been effectively removed. After that, the catalytic performance of FAL aqueous-phase hydrogenation over the acid treated Co@NCNTs-600-800 catalysts has also been investigated and compared with untreated catalyst (Table S3†). It can be found that the activity of treated Co@NCNTs-600-800 catalyst decreased obviously due to the decrease of active Co species.

Different metal catalytic sites usually undergo different reaction pathways, which leads to the different product in the hydrogenation process. To probe the effect of active sites on hydrogenation activity, Ni@NCNTs-600-800 catalyst is synthesized and characterized. Interestingly, we did a series of characterizations, including SEM, TEM, XRD and Raman test (Fig. 6, Fig. S13 and Fig. S14, †). The morphology and microstructure of Ni catalyst was similar to the Co catalyst, indicating that the synthesis strategy can be widely applied to synthesize N-doped carbon nanotubes catalysts with different metal sites. The three sharp peaks at 44.4°, 51.8°, and 76.3° are ascribed to the (111), (002), and (022) of cubic Ni (JCPDS 96-210-0647), respectively (Fig. S13†). Unlike Co-based catalyst, the hydrogenation of furan ring took place over the Ni catalyst, leading to a mixture of FOL, THFOL, and CPO in the product (Fig. S15†). And the FAL conversion and product distribution were high correlated with reaction temperature. FAL conversion gradually raised from 25.8% at 60 ^{o}C to almost 100% at 100 ^{o}C. FOL was major product at the low temperature range (60-70 ^{o}C). The FOL selectivity decreased but THFOL selectivity increased with reaction temperature increased from 80 ^{o}C to 120 ^{o}C. Further increasing reaction temperature, part of FOL was converted to CPO. For instance, the CPO selectivity was 49.4% and the THFOL selectivity was 30.2% when reaction temperature was 150 ^{o}C. Additionally, the time course of reaction was also explored at 100 ^{o}C and 4 MPa H_2 pressure. As shown in Fig. 6c, THFOL selectivity obviously increased with the reaction time, but FOL selectivity decreased correspondingly. It also reveals that the hydrogenation of FAL to THFOL was a consecutive two-step hydrogenation process via the FOL intermediate. Striking, a 99.5% THFOL selectivity with complete conversion could be achieved after 7 h reaction at 100 ^{o}C. Similarly, the step of converting FOL to THFOL could be regarded as the rate-determining step in the aqueous-phase hydrogenation of FAL over the Ni@NCNTs-600-800 catalyst (Fig. S16†). Meanwhile, the TOF values of Ni@NCNTs-600-800 were 27 h^{-1}, 88 h^{-1}, 118 h^{-1} and 160 h^{-1} for temperatures of 90 ^{o}C, 100 ^{o}C, 110 ^{o}C and 120 ^{o}C, respectively (Table S4†).

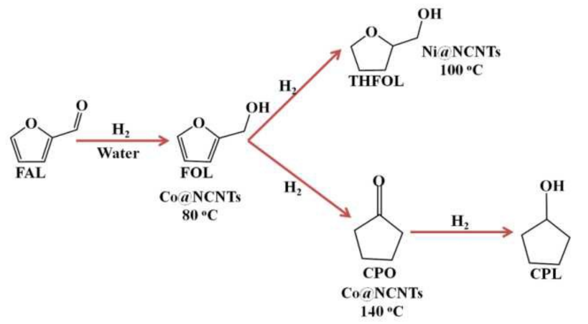

Fig. 7 Reaction pathway for aqueous-phase hydrogenation of FAL over (Co, Ni) based catalysts.

Based on the above experimental results, we suggest a possible pathway for the catalytic aqueous-phase hydrogenation of FAL over Co- and Ni-based catalysts, which is exhibited in Fig. 7. As it shows, FOL is an intermediate in both cases. For the Co-based catalyst, FOL can further convert to CPO via hydrogenation and rearrangement reactions. Meanwhile, the Ni-based catalyst usually converts FOL to THFOL, because metallic Ni nanoparticles are too active and prone to taking place furan ring hydrogenation. The results are in accordance with previous studies.[40, 41]

4. Conclusions

In summary, N-doped carbon nanotubes encapsulated metal (Co, Ni) nanoparticles have been successfully fabricated by a facile pyrolysis approach using melamine as carbon and nitrogen sources. The catalysts showed excellent catalytic performance in aqueous-phase hydrogenation of FAL to some valuable chemicals (FOL, THFOL and CPO). When Co@NCNTs-600-800 was a model catalyst, high yields of FOL (100%) and CPO (75.3%) can be obtained at 80 ^{o}C and 140 ^{o}C, respectively. The catalyst was reused for six cycles without obvious loss of catalytic activity. In addition, a 99.5% THFOL yield can also be attained under 100 ^{o}C reaction temperature and 4 MPa H_2 pressure within 7 h reaction using Ni@NCNTs-600-800 as catalyst. Hence, it provides a universal strategy to construct heterogeneous catalysts for efficient transforming bio-derived platform molecules into important and valuable chemicals.

Conflicts of interest

The authors declare no competing financial interest.

View Article Online
DOI: 10.1039/C8CY01488D

Acknowledgements

This work was financially supported by the National Natural Science Foundation of China (Grant No. 51502297, 51871209, 51372248, and 51432009), Instrument Developing Project of the Chinese Academy of Sciences (Grant No.yz201421).

Notes and references

1 M. Besson, P. Gallezot and C. Pinel, *Chem. Rev.*, 2014, **114**, 1827-1870.
2 D. M. Alonso, S. G. Wettstein and J. A. Dumesic, *Chem. Soc. Rev.*, 2012, **41**, 8075-8098.
3 J. C. Serrano-Ruiz, R. Luque and A. Sepulveda-Escribano, *Chem. Soc. Rev.*, 2011, **40**, 5266-5281.
4 K. Yan, G. Wu, T. Lafleur and C. Jarvis, *Renew. Sust. Energ. Rev.*, 2014, **38**, 663-676.
5 X. Li, P. Jia and T. Wang, *ACS Catal.*, 2016, **6**, 7621-7640.
6 R. Mariscal, P. Maireles-Torres, M. Ojeda, I. Sadaba and M. L. Granados, *Energy Environ. Sci.*, 2016, **9**, 1144-1189.
7 D. Sun, S. Sato, W. Ueda, A. Primo, H. Garcia and A. Corma, *Green Chem.*, 2016, **18**, 2579-2597.
8 S. Bhogeswararao and D. Srinivas, *J. Catal.*, 2015, **327**, 65-77.
9 Y. Liu, Z. Chen, X. Wang, Y. Liang, X. Yang and Z. Wang, *ACS Sustain. Chem. Eng.*, 2017, **5**, 744-751.
10 Y. Nakagawa, M. Tamura and K. Tomishige, *ACS Catal.*, 2013, **3**, 2655-2668.
11 M. M. Villaverde, N. M. Bertero, T. F. Garetto and A. J. Marchi, *Catal. Today*, 2013, **213**, 87-92.
12 M. Ghashghaee, S. Shirvani and M. Ghambarian, *Appl. Catal., A*, 2017, **545**, 134-147.
13 C. P. Jiménez-Gómez, J. A. Cecilia, D. Durán-Martín, R. Moreno-Tost, J. Santamaría-González, J. Mérida-Robles, R. Mariscal and P. Maireles-Torres, *J. Catal.*, 2016, **336**, 107-115.
14 X. Chen, L. Zhang, B. Zhang, X. Guo and X. Mu, *Sci. Rep.*, 2016, **6**, 28558.
15 K. Fulajtárova, T. Soták, M. Hronec, I. Vávra, E. Dobročka and M. Omastová, *Appl. Catal., A*, 2015, **502**, 78-85.
16 Y. Yang, J. Ma, X. Jia, Z. Du, Y. Duan and J. Xu, *RSC Adv.*, 2016, **6**, 51221-51228.
17 M. Hronec, K. Fulajtárová, I. Vávra, T. Soták, E. Dobročka and M. Mičušík, *Appl. Catal., B*, 2016, **181**, 210-219.
18 J. Guo, G. Xu, Z. Han, Y. Zhang, Y. Fu and Q. Guo, *ACS Sustain. Chem. Eng.*, 2014, **2**, 2259-2266.
19 M. Zhou, J. Li, K. Wang, H. Xia, J. Xu and J. Jiang, *Fuel*, 2017, **202**, 1-11.
20 M. Li, F. Xu, H. Li and Y. Wang, *Catal. Sci. Technol.*, 2016, **6**, 3670-3693.
21 M. Li, M. Tang, J. Deng and Y. Wang, *Nano Res.*, 2016, **9**, 3129-3140.
22 D. Su, G. Wen, S. Wu, F. Peng and R. Schloegl, *Angew. Chem. Int. Ed.*, 2017, **56**, 936−964.
23 E. Lam and J. H. T. Luong, *ACS Catal.*, 2014, **4**, 3393-3410.
24 X. Zou, X. Huang, A. Goswami, R. Silva, B. R. Sathe, E. Mikmekova and T. Asefa, Angew. Chem. Int. Ed., 2014, **53**, 4372-4376.
25 J. Meng, C. Niu, L. Xu, J. Li, X. Liu, X. Wang, Y. Wu, X. Xu, W. Chen, Q. Li, Z. Zhu, D. Zhao and L. Mai, *J. Am. Chem. Soc.*, 2017, **139**, 8212-8221..
26 S. Fu, C. Zhu, H. Li, D. Du and Y. Lin, *J. Mater. Chem. A*, 2015, **3**, 12718-12722.
27 T. Cao, D. Wang, J. Zhang, C. Cao and Y. Li, *Chem.*, 2015, **21**, 14022-14029.
28 X. Lin, Z. Nie, L. Zhang, S. Mei, Y. Chen, B. Zhang, R. Zhu and Z. Liu, *Green Chem.*, 2017, **19**, 2164-2173.
29 Y.-Z. Chen, G. Cai, Y. Wang, Q. Xu, S.-H. Yu and H.-L. Jiang, *Green Chem.*, 2016, **18**, 1212-1217.
30 Z. Wei, J. Wang, S. Mao, D. Su, H. Jin, Y. Wang, F. Xu, H. Li and Y. Wang, *ACS Catal.*, 2015, **5**, 4783-4789.
31 E. Yoo, J. Nakamura and H. Zhou, *Energy Environ. Sci.*, 2012, **5**, 6928-6932.
32 D. H. Guo, R. Shibuya, C. Akiba, S. Saji, T. Kondo and J. Nakamura, *Science*, 2016, **351**, 361-365.
33 Z. Li, J. Li, J. Liu, Z. Zhao, C. Xia and F. Li, *ChemCatChem*, 2014, **6**, 1333-1339.
34 W. Gong, C. Chen, H. Zhang, Y. Zhang, Y. Zhang, G. Wang and H. Zhao, *Mol. Catal.*, 2017, **429**, 51-59.
35 Z. Gao, L. Yang, G. Fan, F. Li, *ChemCatChem*, 2016, **8**, 3769-3779.
36 A. Rokicińska, P. Natkański, B. Dudek, M. Drozdek, L. Lityńska-Dobrzyńska and P. Kuśtrowski, *Appl. Catal., B*, 2016, **195**, 59-68.
37 M. G. Dohade and P. L. Dhepe, *Green Chem.*, *2017*, **19**, 1144-1154.
38 M. Audemar, C. Ciotonea, K. De Oliveira Vigier, S. Royer, A. Ungureanu, B. Dragoi, E. Dumitriu and F. Jerome, *ChemSusChem*, 2015, **8**, 1885-1891.
39 X.-L. Li, J. Deng, J. Shi, T. Pan, C.-G. Yu, H.-J. Xu and Y. Fu, *Green Chem.*, 2015, **17**, 1038-1046.
40 Y. Su, C. Chen, X. Zhu, Y. Zhang, W. Gong, H. Zhang, H. Zhao and G. Wang, *Dalton T.*, 2017, **46**, 6358-6365.
41 B. Chen, F. Li, Z. Huang and G. Yuan, *Appl. Catal., A*, 2015, **500**, 23-29.

a

View Article Online
DOI: 10.1039/C8CY01488D

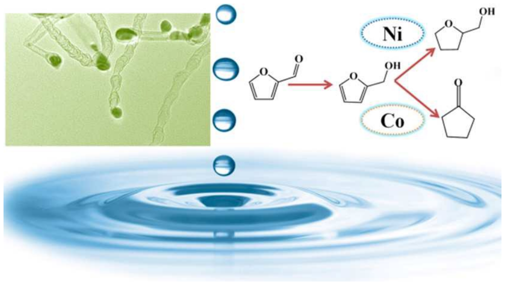

N-doped carbon nanotubes encapsulate (Co, Ni) nanoparticles exhibit excellent catalytic performance for selective reduction of unsaturated oxygen compounds in aqueous-phase